Magnetic excitations in heavy-fermion $CePd_2Si_2$

N. H. van Dijk
Commissariat à l'Energie Atomique, Département de Recherche Fondamentale sur la Matière Condensée, SPSMS, 38054 Grenoble, France
and Delft University of Technology, Interfaculty Reactor Institute, 2629 JB Delft, The Netherlands

B. Fåk and T. Charvolin
Commissariat à l'Energie Atomique, Département de Recherche Fondamentale sur la Matière Condensée, SPSMS, 38054 Grenoble, France

P. Lejay
Centre de Recherches sur les Très Basses Températures, CNRS, BP 166, 38042 Grenoble, France

J. M. Mignot
Laboratoire Léon Brillouin, CEA Saclay, 91191 Gif-sur-Yvette Cedex, France
(Received 14 July 1999; revised manuscript received 30 November 1999)

We have studied the magnetic interactions of single-crystalline $CePd_2Si_2$ by measurements of the electrical resistivity, specific heat, thermal expansion, magnetic susceptibility, and elastic and inelastic neutron scattering. In the paramagnetic phase the system is characterized by Kondo-type spin fluctuations which give rise to a strong quasielastic signal in the inelastic neutron scattering cross section. Below the antiferromagnetic ordering temperature ($T_N = 8.5$ K), the quasielastic signal coexists with spin-wave excitations. The spin waves are strongly dispersive, with a minimum energy of 0.83 meV at the magnetic zone center $\mathbf{k} = (1/2,1/2,0)$. The dispersion can be described in terms of a two-sublattice model with a reduced magnetic exchange interaction and a strong damping of the spin waves due to Kondo screening. The volume dependence of the magnetic interactions has been analyzed using the Grüneisen parameters in order to study the magnetic interactions close to the quantum critical point, which is reached at an applied pressure of about 30 kbar.

I. INTRODUCTION

The magnetic properties of cerium intermetallic compounds are governed by the hybridization of the $4f$ electrons of the Ce ions with the conduction electrons. Depending on the strength of the exchange interaction J either magnetic or nonmagnetic ground states are observed. For small J's, the conduction-electron mediated indirect exchange interaction [Ruderman-Kittel-Kasuya-Yosida (RKKY)] between the $4f$-electron moments dominates, and a magnetic ground state is established. The actual magnetic structure depends on the anisotropy of the RKKY interaction and the anisotropy of the crystal field. With increasing J, screening of the $4f$-electron moments by the conduction electrons (the Kondo effect) becomes more important, resulting in spin fluctuations and a reduced magnetic moment and transition temperature. For a critical value J_c of the exchange interaction, an instability between magnetic and nonmagnetic ground states has been proposed,[1,2] with a second-order zero-temperature phase transition (quantum critical point). For $J > J_c$, a nonmagnetic Fermi-liquid-like state with strong spin fluctuations is established. The widely studied CeT_2Si_2 compounds illustrates this behavior.[3] With a decreasing number of d electrons of the transition-metal element T (or equivalently, decreasing cell volume), the exchange interaction increases, and a transition from localized magnetism with unreduced moments and absence of spin fluctuations to nonmagnetic heavy-fermion systems with strong spin-fluctuation effects and occasionally superconductivity is observed. $CePd_2Si_2$ is a particularly interesting example due to its proximity to a magnetic instability,[4] as seen from the strong pressure dependence of the Néel temperature and from the observation that the Néel and Kondo temperatures are nearly the same.

$CePd_2Si_2$ crystallizes in the body-centered-tetragonal $ThCr_2Si_2$ structure with space group $I4/mmm$. The Hund's rule ground state with $J = 5/2$ of the Ce^{3+} $(4f^1)$ ion is split by the crystal field into three doublets, which have been observed by neutron inelastic scattering.[5,6] Below the Néel temperature $T_N = 8.5$ K, antiferromagnetic order develops with a propagation vector $\mathbf{k} = (1/2,1/2,0)$ and the ordered moments lying in the basal plane.[7,8] The ordered moment of $0.66\mu_B$ is reduced by crystal-field effects and possibly by Kondo screening as well. Kondo-type spin fluctuations develop at low temperatures and give rise to an increase in the density of states at the Fermi level, as manifested in the strong renormalization of the effective mass observed in low-temperature specific-heat measurements, where the linear electronic term is $\gamma \simeq 250$ mJ mol^{-1} K^{-2}.[8] Spin fluctuations are also directly observed in inelastic neutron-scattering experiments.[9,10] The width of the quasielastic spin-fluctuation scattering suggests a Kondo temperature of $T_K \approx 10$ K, i.e., very close to the Néel temperature. This opens up the interesting prospect of studying the magnetic excitations below T_N of a system with strong spin fluctuations. While the dynamic magnetic response due to Kondo spin fluctuations in the paramagnetic state of heavy-fermion cerium compounds is well documented,[11] little is known about the nature of the *mag-*

netic excitations in *ordered* Kondo lattices.

The interplay between the Kondo effect and the RKKY interaction in $CePd_2Si_2$ is nicely illustrated by the strong depression of the Néel temperature with increasing pressure, as observed in resistivity measurements.[12–15] Recently, a superconducting transition with $T_c \approx 0.4$ K was reported[13–15] for pressures around the critical pressure of about 30 kbar. The presence of a superconducting ground state in a limited region around the critical pressure is a strong indication of spin-fluctuation-induced superconductivity.[16] The spin fluctuations are also expected to be responsible for the superconductivity in other heavy-fermion systems and possibly high-T_c superconductors.[17] In addition to the superconducting ground state, the temperature dependence of the normal-state resistivity ($T > T_c$) was found to show significant deviations from the $\rho \propto T^2$ Fermi-liquid behavior. This has lead to speculations that the system may show non-Fermi-liquid properties at the critical pressure, which would confirm recent theoretical predictions.[18–20]

The aim of this work is to characterize the magnetic interactions in $CePd_2Si_2$ by thermodynamic, transport, and neutron-scattering measurements. The paper is organized as follows. Section II describes the results of measurements of the electrical resistivity, specific heat, thermal expansion, and magnetic susceptibility on pieces cut from the same single crystal as used for the neutron-scattering measurements. The latter are dealt with in Sec. III, where we determine the magnetic structure of $CePd_2Si_2$ by the application of an external field and present the results of the inelastic scattering measurements. The main feature is that damped spin-wave excitations coexist with Kondo spin fluctuations in the ordered phase. In Sec. IV we present a crystal-field analysis of the experimental results and discuss the general picture of the magnetic interactions that emerge from the combined effect of crystal-field levels, Kondo fluctuations, and the RKKY interaction. A Grüneisen parameter analysis gives a prediction for the volume dependence of the characteristic energy scales in the system, and has been used to predict the behavior in the proximity to the quantum critical point, which could be at the origin of the unusual physical properties observed in $CePd_2Si_2$.

II. MACROSCOPIC MEASUREMENTS

A. Crystal growth and sample preparation

Polycrystalline $CePd_2Si_2$ was prepared by direct combination of the high-quality elements cerium (4N), palladium (4N), and silicon (6N5). The starting elements with a total weight of nearly 6 g were melted in a water-cooled copper crucible heated by a high-frequency generator under a purified argon atmosphere. To improve homogeneity, the bulk was turned over and remelted several times. The weight loss is negligible using this method to prepare silicides. The material was then introduced in a triarc furnace under inert gas, equipped with a Czochralski puller.[21] The pulling parameters were kept constant during the sample growth (translation speed: 0.5 cm/h; seed-rotation speed: 30 rpm; crucible-rotation speed: 20 rpm). The bulk materials were checked by conventional x-ray powder diffraction and the single crystalline state was confirmed using back-scattering x-ray Laue technique. Microprobe analysis (CAMEBAX SX) performed along the growth direction revealed homogeneous samples with the right composition, without any trace of parasitic phases. The single crystals were annealed in a resistive ultrahigh-vacuum furnace for 8 days at 950 °C under a pressure of 3.5×10^{-10} torr. The structure was checked with Rietveld analysis from the x-ray pattern (crushed part of the growth). The fit confirmed the $ThCr_2Si_2$-type structure space group $I4/mmm$ with Ce, Pd, and Si, respectively, on $2a$, $4d$, and $4e$ ($z = 0.3778$) sites. The lattice parameters are $a = 4.2318$ Å and $c = 9.9035$ Å.

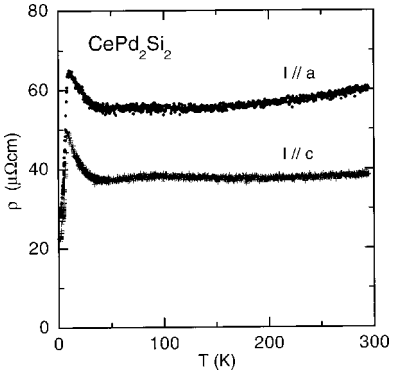

FIG. 1. Electrical resistivity ρ of $CePd_2Si_2$ as a function of temperature for a current I along the crystallographic a axis (solid circles) and c axis (pluses).

Two single crystals in the shape of cylinders with masses of 2.3 g (crystal A) and 1.9 g (crystal B) were used in our experiments. Part of the neutron-scattering experiments were performed on the two combined crystals, while other neutron experiments were done on only one of the crystals (B) for comparison. Crystal A, which was also used in earlier neutron-scattering experiments,[22] was subsequently used to prepare samples for measurements of the resistivity, specific heat, thermal expansion, and susceptibility.

B. Electrical resistivity

The electrical resistivity of $CePd_2Si_2$ was measured with a four-point ac technique on two single-crystalline samples (crystal A) with characteristic dimensions of $1 \times 1 \times 4$ mm^3 cut along the a and c axis, respectively. Figure 1 shows the temperature dependence of the electrical resistivity. At low temperatures, the upturn in the electrical resistivity for both directions is related to Kondo scattering. At $T_N = 8.5$ K, the system orders antiferromagnetically and a reduction in the electrical resistivity is observed. A broad maximum around 100 K signals additional scattering from crystal-field excitations. The residual resistivities of 27 $\mu\Omega$ cm (a axis) and 21 $\mu\Omega$ cm (c axis) are similar to earlier measurements.[8,23]

C. Specific heat

The specific heat of $CePd_2Si_2$ was measured by a dynamic adiabatic method on a single-crystalline sample (crystal A) with a mass of 50 mg. Figure 2 shows the specific heat c as a function of temperature. At the antiferromagnetic transition ($T_N = 8.5$ K) a jump in the specific heat is observed. A comparison with the specific heat of the nonmagnetic reference system $LaPd_2Si_2$ indicates the presence of a crystal-field contribution with a maximum at 90 K.[24] The magnetic

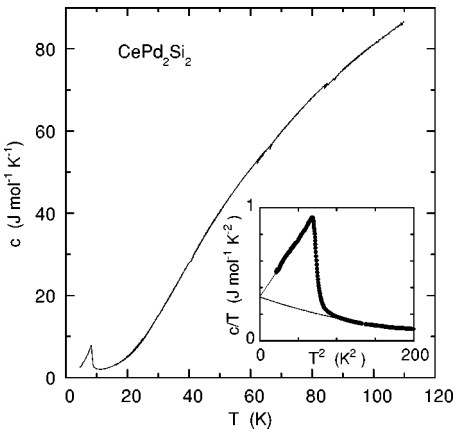

FIG. 2. Specific heat c as a function of temperature for $CePd_2Si_2$. The inset shows the magnetic contribution of c/T as a function of T^2 after subtraction of the reference data for $LaPd_2Si_2$ from Ref. 24. The lines in the inset are low-temperature extrapolations of the specific-heat contributions from the spin fluctuations and the spin waves.

contribution of the $4f$ electrons at low temperatures is obtained after subtraction of the data for $LaPd_2Si_2$. In the inset of Fig. 2, the magnetic contribution of c/T is shown as a function of T^2. In the paramagnetic phase an increase in c/T is observed for decreasing temperature, which is due to Kondo spin fluctuations. The specific heat in the antiferromagnetically ordered state can be described in terms of spin fluctuations and an additional spin-wave contribution. The spin-wave contribution can empirically be described by a T^3 power law. In the low-temperature limit, the spin-wave contribution vanishes and the specific heat is dominated by the spin fluctuations with an enhanced linear term of $\gamma_0 \approx 330$ $\mathrm{mJ\,mol^{-1}\,K^{-2}}$, as obtained by extrapolation[8] of the data shown in the inset of Fig. 2. A comparison with the linear term at T_N ($\gamma \approx 200$ $\mathrm{mJ\,mol^{-1}\,K^{-2}}$) indicates a significant temperature dependence of the spin fluctuations in the antiferromagnetically ordered state, as expected for the relatively low Kondo temperature of $T_K \approx 10$ K.[9,24]

D. Thermal expansion

The thermal expansion of $CePd_2Si_2$ was measured with a sensitive three-terminal parallel-plate capacitance technique.[25] The dilatation was measured along the a and c axes of a single-crystalline sample (crystal A) with dimensions $1.5\times1.5\times3$ $\mathrm{mm^3}$ ($=a\times a\times c$). Figure 3 shows the coefficient of the linear thermal expansion $\alpha=(1/L)(dL/dT)$ for temperatures up to 200 K. At high temperatures the coefficient of the linear expansion along the a axis shows a Debye temperature dependence, characteristic for the phonon contribution. The upturn in α_a below 30 K signals the development of spin fluctuations. At the antiferromagnetic transition ($T_N=8.5$ K) a large step in α_a with a change of sign is observed. The coefficient of the linear thermal expansion along the c axis shows an unusual temperature dependence. At high temperatures, α_c is negative and shows a large minimum around 100 K, which can be attributed to the crystal-field contribution. At the antiferromagnetic transition a large step in α_c with a change of sign is observed. The coefficient

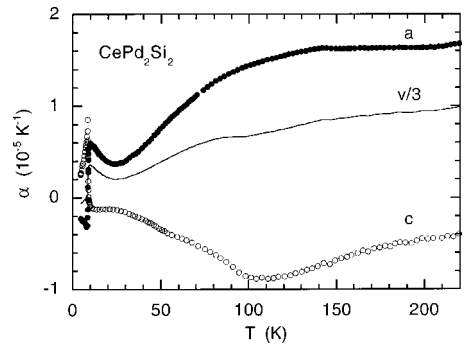

FIG. 3. Temperature dependence of the linear thermal-expansion coefficient α of $CePd_2Si_2$ along the a axis (solid circles) and c axis (open circles), and of the volume thermal-expansion coefficient (line).

of the volume thermal expansion $\alpha_v=(1/V)(dV/dT)=2\alpha_a+\alpha_c$ is positive at high temperatures and nearly vanishes below T_N.

E. Susceptibility

The dc magnetic susceptibility of $CePd_2Si_2$ was measured with a commercial Quantum Design superconducting quantum interference device in magnetic fields up to 5.5 T. Three samples (crystal A) with a mass of 0.1 g were cut along the [100], [110], and [001] directions. Figure 4 shows the measured susceptibility as a function of temperature in a magnetic field of $B=2$ T ($B\|a$ and $B\|c$). A remarkable change in the easy direction is observed around 50 K. At high temperatures the c axis is the easy axis while at low temperatures the basal plane acts as the easy direction. The high-temperature susceptibility can be described in terms of a Curie-Weiss temperature dependence with $\theta_a=-47$ K ($B\|a$) and $\theta_c=-18$ K ($B\|c$) and the free-moment value of $2.54\mu_B$ for the effective moment. In Fig. 5 the low-temperature susceptibility as function of temperature is

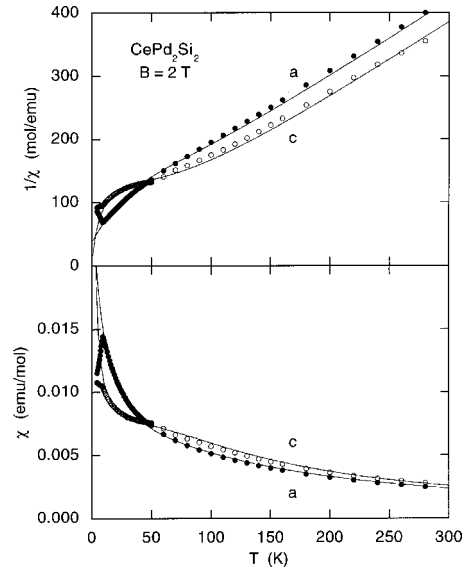

FIG. 4. Temperature dependence of the magnetic susceptibility χ (and its inverse) of $CePd_2Si_2$ in a magnetic field of 2 T along the a (solid circles) and c axis (open circles). The lines are fits as described in the text.

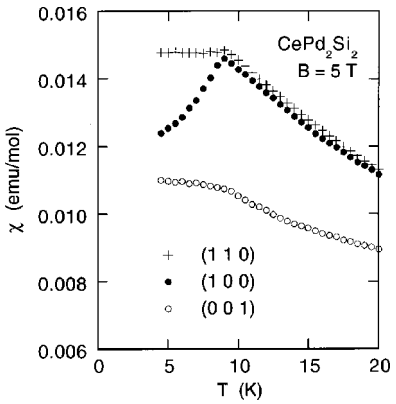

FIG. 5. Low-temperature susceptibility χ of $CePd_2Si_2$ as a function of temperature in a magnetic field of 5 T along the directions [100] (solid circles), [110] (pluses), and [001] (open circles).

shown. At the antiferromagnetic transition ($T_N = 8.5$ K) a kink is observed for magnetic fields along the a and the c axis. The difference in behavior between the two basal-plane directions [100] and [110] reflects the presence of two magnetic domains, as evidenced by neutron-scattering measurements (see Sec. III A).

III. NEUTRON-SCATTERING MEASUREMENTS

Neutron-scattering measurements were performed on the cold-neutron triple-axis spectrometers IN12 at the high-flux reactor of Institut Laue-Langevin and 4F2 at the Orphée reactor (Laboratoire Léon Brillouin). Several different configurations were tested in order to optimize the measurement conditions and to rule out spurious effects. In all cases, pyrolytic graphite (002) planes were used as monochromator and analyzer, with the monochromator being vertically focused and the analyzer flat or horizontally focused. Most measurements were done with a fixed final wave vector. On 4F2, a 4-cm thick pyrolytic graphite filter was used in the scattered beam to reduce higher-order contributions, while no filter was needed on IN12 due to the guide cutoff. The principal configurations used are listed in Table I. The two single crystals (A and B) were mounted together with either the [001] axis or the [1,−1,0] axis vertical, in a standard (orange) helium-flow cryostat or in a vertical-field superconducting magnet. Some measurements were performed on only one of the crystals (B) to eliminate spurious effects. The data for the inelastic neutron-scattering measurements were normalized to the beam monitor (after correction for higher-order contamination), a flat background (determined at negative energy transfers) was subtracted, and points within 0.4 meV from the elastic peak were excluded due to the strong incoherent elastic scattering. The energy resolution for configurations A and C is 0.26 meV.

TABLE I. Principal triple-axis spectrometer configurations used.

Configuration	Instrument	k_f (Å^{-1})	Analyzer	Collimation (min)	Filter
A	4F2	1.64	Focused	Open	PG
B	4F2	1.97	Focused	Open	PG
C	IN12	1.81	Flat	29-43-43-60	None

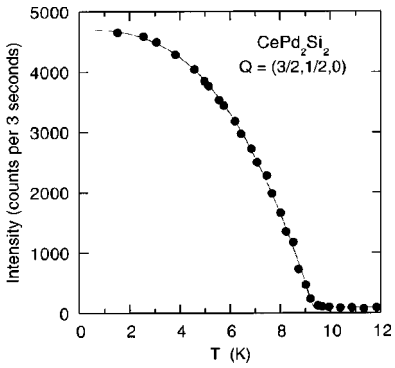

FIG. 6. Temperature dependence of the magnetic Bragg peak intensity of $CePd_2Si_2$ at $\mathbf{Q}=(3/2,1/2,0)$. Statistical errors are smaller than the symbol size. The line is a fit to Eq. (1).

A. Elastic scattering

The magnetic order of $CePd_2Si_2$ is characterized by a propagation vector of $\mathbf{k}=(1/2,1/2,0)$ and the absence of a magnetic Bragg reflection at $\mathbf{Q}=(1/2,1/2,0)$, which means that the Fourier components $\mathbf{m_k}$ of the moment are parallel to the $\mathbf{k}$ vector. The peak intensity of the magnetic Bragg scattering at $\mathbf{Q}=(3/2,1/2,0)$, measured in configuration B, is shown as a function of temperature in Fig. 6. The temperature dependence is well described by the empirical relation

$$I(T)=I_0[1-(T/T_N)^{\alpha}]+b, \tag{1}$$

where I_0 is proportional to the moment squared, $T_N = 9.30(2)$ K, $\alpha = 2.72(5)$, and b is the background. The critical exponent β obtained by fitting the peak intensity close to T_N to the expression

$$I(T)=I_0(1-T/T_N)^{2\beta}+b, \tag{2}$$

takes the mean-field value of 0.5, in agreement with early measurements.[7] Detailed measurements even closer to the antiferromagnetic transition temperature indicate a somewhat lower value of $\beta = 0.37$.[8]

The magnetic structure is not unambiguously determined by the observed magnetic Bragg reflections. The two propagation vectors $\mathbf{k}=(1/2,1/2,0)$ and $\mathbf{k}=(1/2,-1/2,0)$ can either correspond to a single-$\mathbf{k}$ structure with moments along the [110]-type directions and 2 magnetic domains or a double-$\mathbf{k}$ structure with moments along the [100]-type directions. In order to distinguish between these two structures, we have measured the (1/2,1/2,2) magnetic Bragg peak in configuration C with a magnetic field applied along the [1,−1,0] direction. In a double-$\mathbf{k}$ structure, no change is expected in the Bragg intensity, while a domain repopulation is expected to increase the intensity for a single-$\mathbf{k}$ structure. Figure 7 shows that the intensity increases by a factor of 2 for an applied magnetic field of 4 T, which proves that the structure is single $\mathbf{k}$. The presence of a single-$\mathbf{k}$ structure is further supported by the difference in magnetic susceptibility for magnetic fields along the [100] and [110] directions (Fig. 5). We, therefore, conclude that the antiferromagnetically ordered structure is in agreement with the earlier reported

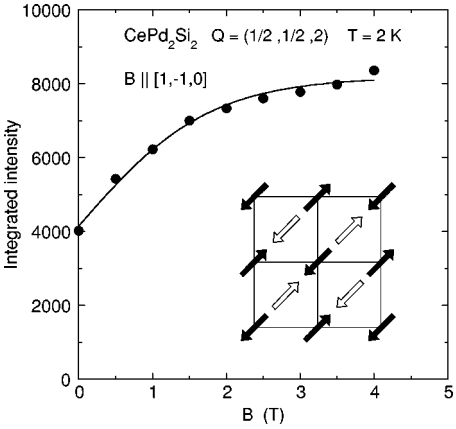

FIG. 7. Magnetic Bragg peak intensity of $CePd_2Si_2$ at $\mathbf{Q}=(1/2,1/2,2)$ as a function of external field. The statistical errors are of the size of the symbols. The line is a fit to Eq. (3). The inset shows the magnetic structure of $CePd_2Si_2$ for one domain, projected onto the basal plane.

structure of Refs. 7 and 8. A sketch of the ordered structure of one of the domains is shown in Fig. 7.

The solid line in Fig. 7 is a fit of the domain repopulation as a function of magnetic field B to the empirical relation

$$I(B)=\frac{2I_0}{1+\exp(-cB/T)}, \tag{3}$$

where c is a constant. The magnitude of the ordered moment, obtained by normalizing the magnetic Bragg reflections to the weak nuclear $\mathbf{Q}=(110)$ reflection, amounts to $0.80(5)\mu_B$. This value is somewhat higher than that from earlier neutron-diffraction experiments, $0.66\mu_B$,[7,8] but smaller than the value of $0.94\mu_B$, reported from nuclear magnetic resonance measurements.[26]

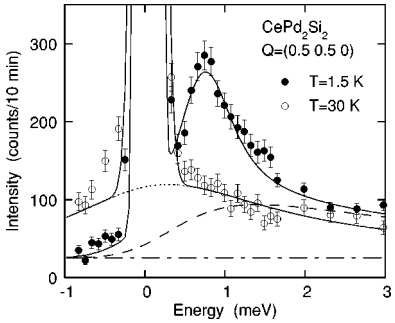

FIG. 9. Energy scan at $\mathbf{Q}=(1/2,1/2,0)$ for $T=1.5$ K (solid circles) and $T=30$ K (open circles). Raw data is shown, i.e., before background and elastic peak subtraction, but after normalization to the monitor. The dotted (dashed) line shows the quasielastic contribution at high (low) temperatures and the dash-dotted line shows the estimated background level. The total fitted contribution (elastic peak, quasielastic contribution, and, at $T=1.5$ K, the spin wave) is shown by the solid lines.

B. Inelastic scattering

Figure 8 shows typical energy scans for different wave vectors at $T=1.5$ K in the antiferromagnetic phase of $CePd_2Si_2$. Near the antiferromagnetic zone center $\mathbf{Q}_{\rm afm}=(1/2,1/2,0)$, there is a clear inelastic peak which corresponds to a somewhat damped spin-wave excitation. The long tail of the scattering *cannot* be accounted for by resolution broadening of the spin waves. It corresponds actually to a broad quasielastic contribution. As the wave vector goes away from $\mathbf{Q}_{\rm afm}$, the spin-wave energy increases and the damping becomes very important. In the paramagnetic phase, only the quasielastic scattering remains, as shown in Fig. 9.

The characteristic feature of the spin dynamics in $CePd_2Si_2$ is the coexistence of Q-independent Kondo-type fluctuations and dispersive spin waves in the antiferromagnetically ordered state. The latter are strongly damped away

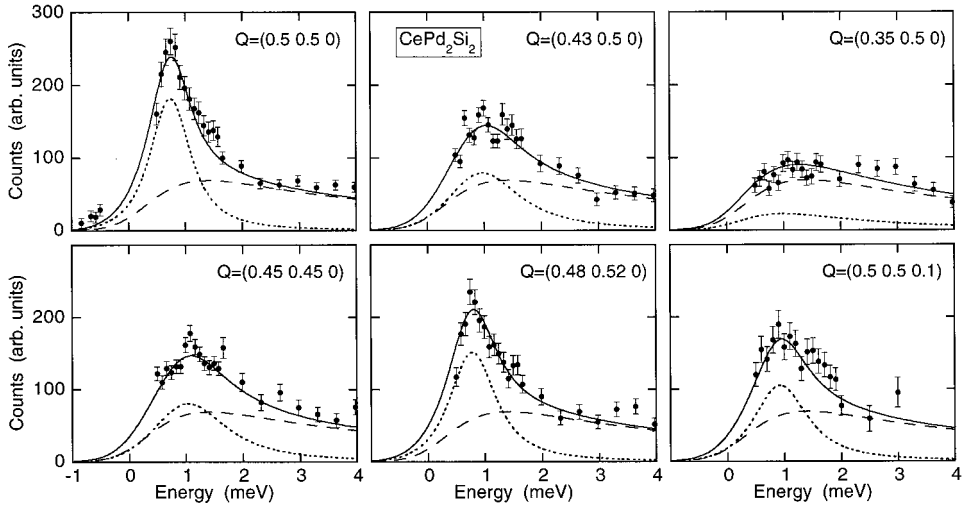

FIG. 8. Typical energy scans at different wave vectors near $\mathbf{Q}_{\rm afm}=(1/2,1/2,0)$ at $T=1.5$ K in the antiferromagnetically ordered phase of $CePd_2Si_2$. (a)–(e) Measured in configuration A (see Table I) without any applied field. (f) Measured in configuration C with an applied field of 4 T along the $[1\ -1\ 0]$ axis. The solid line is a fit of Eq. (4) convoluted with the instrumental resolution. The Q-independent quasielastic contribution is shown by the dashed line, and the spin-wave contribution by the dotted line. For clarity, the background and the elastic peak have been removed.

from the magnetic zone center. Experimentally, it is difficult to obtain a unique separation of the two contributions, since both are broad in energy with similar energy scales ($T_N \approx T_K \approx 10$ K). In addition, the existence of two magnetic domains doubles the number of spin-wave modes for a given **Q** vector. In the following we will first describe the method used to separate the different contributions, and then discuss the obtained results.

The application of an external field of 4 T ($B \| [1,-1,0]$) gives a nearly complete depopulation of one of the magnetic domains, as seen from the magnetic Bragg peak intensity (Fig. 7), and discussed above. On the other hand, no change is seen in the spin-wave scattering, except for a field-induced increase of the energy gap by 0.1 meV and a small change in intensity. The line shape remains the same, which means that the contribution from the second domain is negligible close to the magnetic zone center of the first domain. This is certainly related to the strong damping of the spin-wave scattering away from the zone center.

The inelastic neutron-scattering data can be described as a sum of two contributions,

$$S(\mathbf{Q},\omega) = \frac{1}{1-\exp(-\hbar\omega/k_BT)} \times \left[\frac{\chi_L \omega \Gamma_L}{\omega^2+\Gamma_L^2} + \frac{\chi_{\mathbf{Q}} 2\omega\Omega_{\mathbf{q}}^2 \Gamma_{\mathbf{q}}}{(\omega^2-\Omega_{\mathbf{q}}^2)^2+4\omega^2\Gamma_{\mathbf{q}}^2} \right], \quad (4)$$

where the first term in the brackets is a Lorentzian function describing the Q-independent quasielastic Kondo-type spin fluctuations with characteristic relaxation rate Γ_L^{-1}, and the second term is a damped harmonic oscillator (DHO) used for the spin waves with a propagation vector **q** [with respect to the antiferromagnetic zone center $\mathbf{Q}=(1/2,1/2,0)$]. These two functions are multiplied by the temperature factor and convoluted with the instrumental resolution function. Due to the difficulties of separating these two contributions (one **Q** dependent and the other not), Eq. (4) was fitted simultaneously to data taken at several different **Q** vectors close to the antiferromagnetic zone center, including different symmetry directions. To further improve the precision in the fits (and reduce the number of fitted parameters), the **q** dependence of the DHO in Eq. (4) was parametrized in the following way. The spin-wave damping was found to be isotropic and well described by the empirical relation $\Gamma_q = \Gamma_0 + Dq^2$, where Γ_0 (= 0.4 meV) and D are constants. The susceptibility $\chi_{\mathbf{Q}}$ was well described by a Lorentzian q dependence,

$$\chi_{\mathbf{Q}} = \frac{\chi_{\mathrm{AFM}}}{1+(q_\perp/\kappa_\perp)^2+(q_\parallel/\kappa_\parallel)^2}, \quad (5)$$

where χ_{AFM} is the susceptibility at the zone center, $q_\perp$ is the distance of the wave vector **Q** from (1/2,1/2,0) in the tetragonal a-b plane, $q_\parallel$ is the distance along the c^* axis, and $\kappa_\perp$ and $\kappa_\parallel$ are the corresponding correlation lengths. The spin-wave energy was fitted to a spin-wave model discussed below (Sec. III D), which has three parameters: two exchange interactions J_1 and J_2 and a molecular-field term H_M. A typical fit thus contains nine parameters (χ_L, Γ_L, D, χ_{AFM}, $\kappa_\perp$, $\kappa_\parallel$, J_1, J_2, and H_M) and 360 data points representing 15 different **Q** vectors (configurations A and C). These **Q** vectors are typically within 0.2 Å^{-1} from the magnetic zone center, since no well-defined spin waves are observed further away. This also assures that contributions from the second domain remain negligible. Typical fits are shown in Fig. 8.

C. Spin fluctuations

Measurements on polycrystalline samples in the paramagnetic phase show quasielastic scattering with a characteristic energy of the form $\Gamma(T) = \Gamma(0) + cT^{1/2}$, typical for local Kondo-type spin fluctuations.[9] The line width at T_N is of the order of 0.9 meV, which was interpreted as a Kondo temperature of $T_K \approx 10$ K.[9] Our measurements on single crystals indicate that these fluctuations are Q independent, as expected for local spin fluctuations. We find a somewhat larger width of 1.6 meV at a temperature of $T = 30$ K, which compares to 1.1 meV for polycrystalline samples.[9] We do not believe this difference is significant, due to the difficulty of subtracting the phonon contribution in single-crystal work. Below T_N, the line width decreases as expected from the increased linear term in the specific heat, and we find from our fits at $T = 1.5$ K a value of about 1.4 meV, although smaller widths (down to 1 meV) are still compatible with our data. The temperature dependence of the excitation spectrum at the antiferromagnetic zone center is shown in Fig. 9. We find that the quasielastic integrated intensity (χ_L) increases below T_N, by nearly a factor of 2.

D. Spin waves

The spin-wave dispersion of an antiferromagnet can be described in terms of a simplified two-sublattice model,[27]

$$\mathcal{H} = -\sum J(\mathbf{r})\, \mathbf{S_n} \cdot \mathbf{S_{n+r}} - g\mu_B H_M \sum S_n^z, \quad (6)$$

where $J(\mathbf{r})$ describes the antiferromagnetic exchange interactions between the sublattices, and all the ferromagnetic exchange interactions within the sublattice are approximated by an effective molecular field H_M in order to restrict the number of model parameters. For $CePd_2Si_2$, the former is dominated by the nearest-neighbor interaction $J_1 = J(\pm a,0,0) = J(0,\pm a,0)$ and the next-nearest-neighbor interaction $J_2 = J(a/2,a/2,\pm c/2) = J(-a/2,-a/2,\pm c/2)$ in the $\mathbf{k} = (1/2,1/2,0)$ domain. The next-nearest-neighbor interaction J_2 is essential to describe the preferred spin orientation of the moments. The spin-wave dispersion for this model is given by[27]

$$\Omega(\mathbf{q}) = \{[g\mu_B H_M - 2SJ(0)]^2 - [2SJ(\mathbf{q})]^2\}^{1/2}, \quad (7)$$

where

$$J(\mathbf{q}) = \sum J(\mathbf{r}) \exp(-i\mathbf{q}\cdot\mathbf{r}) = 2J_1[\cos(2\pi q_x) + \cos(2\pi q_y)] + 4J_2 \cos[\pi(q_x+q_y)]\cos(\pi q_z), \quad (8)$$

and $\mathbf{q} = (q_x, q_y, q_z)$ is given in reduced lattice units with respect to the antiferromagnetic zone center. Near the magnetic zone center $\mathbf{q} = 0$, the dispersion is quadratic in q with

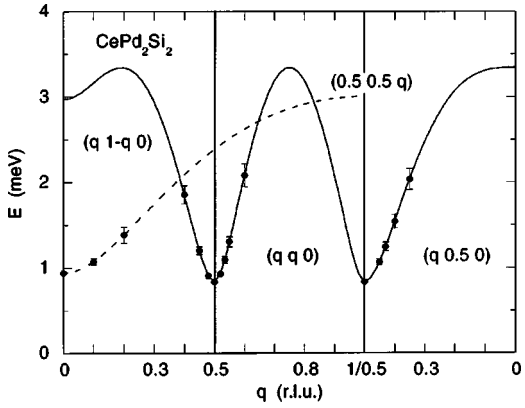

FIG. 10. Dispersion curve for the antiferromagnetic spin waves in $CePd_2Si_2$ at $T=1.5$ K. The solid line shows the dispersion in the basal plane without any applied field (configuration A; see Table I) and the dashed line is the dispersion along the tetragonal axis in a field of 4 T applied along the $[1\ -1\ 0]$ axis (configuration C). The dispersion curves are obtained by fitting Eqs. (4) and (7–8) to the measured data at **Q** values shown by the solid circles. The error bars represent the error in the spin-wave energy arising from the uncertainties in the fitted parameters H_M, J_1, and J_2.

a minimum energy of $\Delta=\Omega(0)=\{g\mu_B H_M[g\mu_B H_M - 4SJ(0)]\}^{1/2}$, where, from Eq. (8), $J(0)=4(J_1+J_2)$.

In our fits to the data, the spin-wave energy $\Omega_{\mathbf{q}}$ was described by Eqs. (7) and (8). The measured dispersion for the directions [110], [100], [1−10], and [001] are well described in terms of this simple two-sublattice model, as shown in Fig. 10. We found a gap energy Δ of 0.83 meV in zero field and 0.94 meV in a field of 4 T. The fitted exchange interaction is $2S(J_1+J_2)=-0.81$ meV and the molecular field is $g\mu_B H_M=0.11$ meV. Since the spin waves die out rapidly in the c direction, it is difficult to obtain good estimates for the ratio of the nearest-neighbor interaction J_1 and the next-nearest-neighbor interaction J_2, but the data suggest that J_2 is quite substantial, with typical estimates being $J_2/J_1\sim 1/3$. The values quoted here differ somewhat from those in a preliminary report,[28] where a subset of the present data was fitted for individual **Q** values. Also, the characteristic spin-wave energy is here taken as $\Omega_{\mathbf{q}}=(\omega_{\mathbf{q}}^2+\Gamma_{\mathbf{q}}^2)^{1/2}$, while $\omega_{\mathbf{q}}$ was used in Ref. 28. At $\mathbf{q}=0$, we have $\Delta=\Omega_0=0.83$ meV and $\Gamma_0=0.4$ meV, which corresponds to $\omega_0=0.73$ meV, in good agreement with Ref. 28.

The intensity of the spin waves decreases rapidly as **Q** goes away from the magnetic zone center, given by Eq. (5), with correlation lengths of $\kappa_\perp=0.12$ (1) Å^{-1} and $\kappa_\parallel=0.08$ (1) Å^{-1}. This intensity drop away from the magnetic zone center is due to a damping of the spin waves by the strong spin fluctuations. This damping is also reflected by the intrinsic width Γ_q of the spin waves, which also increases with q. The combined effect is such that no propagating spin waves are observed for wave vectors that are more than 0.2 Å^{-1} away from the magnetic zone center. The parameters obtained from the fits to the quasielastic spin fluctuations and the inelastic spin waves are summarized in Table II.

IV. DISCUSSION

A. Crystal fields

The crystal-field Hamiltonian for Ce^{3+} ($J=5/2$) in a field with tetragonal point symmetry can be expressed as[29,30]

$$\mathcal{H}_{\mathrm{CF}}=B_2^0\mathbf{O_2^0}+B_4^0\mathbf{O_4^0}+B_4^4\mathbf{O_4^4}, \tag{9}$$

where the c axis is taken as the quantization axis, $\mathbf{O_j^i}$ are the Stevens operators, and B_j^i the crystal-field parameters of the Ce^{3+} ion. The eigenfunctions of the Hamiltonian Eq. (9) are

$$\begin{aligned}\Gamma_{t7}^{(2)}&=a|\pm 5/2\rangle+b|\mp 3/2\rangle,\\ \Gamma_{t7}^{(1)}&=b|\pm 5/2\rangle-a|\mp 3/2\rangle,\\ \Gamma_{t6}&=|\pm 1/2\rangle.\end{aligned} \tag{10}$$

Inelastic neutron-scattering measurements on $CePd_2Si_2$ show two crystal-field excitations at 19 and 24 meV between the lowest doublet and the two excited doublets.[5,6] The crystal-field contribution, observed in the electrical resistivity, the specific heat,[24] and the thermal expansion, confirm the characteristic energy scale of the excited levels. The susceptibility measurements show a rather unusual temperature dependence with a change in the magnetic anisotropy at 50 K. At high temperatures the c axis is the easy axis, while below 50 K the easy direction for the magnetization lies within the basal plane. In the antiferromagnetically ordered phase the ordered moments are oriented along the ordering vector $\mathbf{k}=(1/2,1/2,0)$, which corresponds to the easy axis. When the two antiferromagnetic domains are equally populated, the system has two easy axes and qualitatively behaves as an easy-plane system. The magnetic anisotropy of the ordered state is also observed in the paramagnetic state below 50 K, as shown in the static susceptibility of Fig. 4.

The unusual ordering vector $\mathbf{k}=(1/2,1/2,0)$ below T_N suggests that the B_4^4 parameter is positive and behaves as the dominant crystal-field parameter. The crystal-field excitation spectra, determined from inelastic neutron-scattering measurements,[5,6] were interpreted in terms of a set of negative crystal-field parameters. These parameters were later refined with additional magnetic-susceptibility measurements.[31] As discussed by Hippert and co-workers,[22] the corresponding easy-axis magnetic anisotropy along the c axis does not correspond to the susceptibility measurements and the ordering vector $\mathbf{k}=(1/2,1/2,0)$ in the antiferromag-

TABLE II. Fitting parameters for the quasielastic spin fluctuations and the inelastic spin waves at $T=1.5$ K and zero field.

	Γ_L	D	$\kappa_\parallel$	$\kappa_\perp$	$2S(J_1+J_2)$		$g\mu_B H_M$
$\chi_L/\chi_{\mathrm{AFM}}$	(meV)	(meV Å^2)	(Å^{-1})	(Å^{-1})	(meV)	J_2/J_1	(meV)
0.8	1.4	0.4	0.08	0.12	−0.81	∼1/3	0.11

netic phase. Instead, Hippert and co-workers derived an alternative set of crystal-field parameters[32] for an isotropic (Heisenberg) magnetic exchange interaction, which reproduces the magnetic anisotropy for the susceptibility and predicts the proper magnetic structure below T_N.

In order to take into account the anisotropy of the magnetic exchange interaction we used a slightly different approach than Hippert and co-workers.[22] First, the energy splitting between the lowest doublet and the two excited doublets was fixed at the values determined by Steeman *et al.*: $\Delta_1 = 19$ meV and $\Delta_2 = 24$ meV.[6] The remaining crystal-field parameter was used as a free parameter to reproduce the temperature dependence of the inverse susceptibility $1/\chi = 1/\chi_{\mathrm{CEF}} - \lambda$, where the magnetic exchange interactions were taken into account with an anisotropic molecular field λ. The best fit to the measured susceptibility was obtained with crystal field parameters of $B_2^0 = 0.044$ meV, $B_4^0 = 0.041$ meV, and $B_4^4 = 0.401$ meV and molecular fields of $\lambda_a = -30$ mol/emu for the basal plane and $\lambda_c = 5$ mol/emu for the c axis. The crystal-field parameters are dominated by B_4^4, which shows the proper magnetic anisotropy for the ordering vector $\mathbf{k} = (1/2,1/2,0)$ below T_N, while B_2^0 is relatively small. The change in the magnetic anisotropy at 50 K arises from the magnetic exchange interaction, described by the anisotropic molecular field, which is antiferromagnetic in the plane and slightly ferromagnetic along the c axis. The level scheme for these crystal-field parameters is

$$24 \text{ meV} = = = = = = a|\pm 5/2\rangle + b|\mp 3/2\rangle,$$

$$19 \text{ meV} = = = = = = |\pm 1/2\rangle,$$

$$0 \text{ meV} = = = = = = b|\pm 5/2\rangle - a|\mp 3/2\rangle.$$

The mixing parameters of the J_z states correspond to $a = 0.849$ and $b = 0.529$. These values are relatively close to the values obtained by Steeman *et al.*[6] from the relative intensities of the crystal-field excitations in the inelastic neutron-scattering measurements. The effective moment of $0.86\mu_B$, calculated from the crystal-field parameters, accounts for most of the moment reduction at low temperatures. The effect of the moment reduction is nicely demonstrated in high-field magnetization measurements, where no transition was observed for applied magnetic fields up to 28 T along the a and the c axes.[33]

B. Magnetic order

Elastic neutron scattering and susceptibility measurements confirmed that the magnetic structure of $CePd_2Si_2$ corresponds to antiferromagnetic order with a single propagation vector. In the absence of an applied magnetic field, magnetic domains with propagation vectors $\mathbf{k} = (1/2,1/2,0)$ and $\mathbf{k} = (1/2,-1/2,0)$ are formed. An applied magnetic field along the propagation vector of one of the domains induces a domain repopulation, as is clearly demonstrated in the elastic neutron-scattering measurements. The susceptibility measurements of Fig. 5 show a pronounced anisotropy, which is consistent with a (nearly) complete domain repopulation for $B \| [110]$. In the antiferromagnetically ordered state a remarkable coexistence of spin fluctuations and spin waves is observed in the inelastic neutron-scattering measurements. The spin-wave dispersion shows a finite excitation gap of 0.83 meV at the magnetic zone center $\mathbf{k} = (1/2,1/2,0)$. A strong competition between the antiferromagnetic order and the spin fluctuations is suggested by the strong damping of the spin-wave excitations away from the magnetic zone center. The temperature dependence of the specific heat, thermal expansion, and the variation in the ordered moment is well described by a power-law behavior, characteristic for a gapless antiferromagnet. This is a remarkable observation since the spin-wave dispersion shows a sizable excitation gap, and therefore, a more complicated temperature dependence is expected.[34]

The spin-wave dispersion, determined from the inelastic neutron-scattering measurements, can accurately be described by a simple two-sublattice model as shown in Fig. 10. The magnetic interactions have been modeled with three parameters: the nearest-neighbor interaction J_1 and the next-nearest-neighbor interaction J_2 for the interactions between the sublattices, and an effective molecular field H_M for the interactions within one sublattice. The magnetic interaction between the sublattices is antiferromagnetic for both the nearest-neighbor and the next-nearest-neighbor interaction. The relative strength of the next-nearest-neighbor interaction $J_2/J_1 \sim 1/3$ is small but significant for the magnetic structure of the antiferromagnetic order. The effective molecular field of the magnetic interactions is ferromagnetic, as expected from the magnetic structure. The relative strength of the ferromagnetic interactions compared to the antiferromagnetic interactions is $g\mu_B H_M/[2S(J_1+J_2)] = -0.14$. The magnetic structure derived from the model description of the dispersion is in qualitative agreement with the crystal-field calculations of the magnetic susceptibility, where an anisotropic molecular field was obtained with a relative strength of $\lambda_c/\lambda_a = -0.17$.

C. Grüneisen parameters

1. Crystal field

The thermal expansion along the c axis is negative above T_N and shows a pronounced minimum around 100 K. The corresponding crystal-field splitting amounts to $\Delta_{\mathrm{CEF}} \approx 21$ meV for a Schottky peak. This is in qualitative agreement with the presence of two excited crystal-field doublets at 19 and 24 meV, observed by inelastic neutron-scattering measurements. The thermal expansion along the a axis does not reveal a significant deviation from the phonon contribution around 100 K, indicating that the crystal-field contribution is at least one order of magnitude smaller along the a axis. The volume dependence of the crystal-field splitting can be estimated from the Grüneisen parameter $\Gamma_{\mathrm{CEF}} = -d \ln \Delta_{\mathrm{CEF}}/d \ln V = V_m \alpha_v/\kappa c$, where $V_m = 5.31 \times 10^{-5}$ $\mathrm{m}^3/\mathrm{mol}$ is the molar volume and $\kappa = -(1/V)(dV/dp)$ the isothermal compressibility. The experimental thermal expansion at the minimum near 100 K is $\alpha_v \approx \alpha_c = -8.9 \times 10^{-6}$ K^{-1}, while the calculated specific heat for two excited doublets at 19 and 24 meV has a maximum of $c = 6.2$ $\mathrm{J\,mol^{-1}\,K^{-2}}$. A careful analysis of the specific-heat

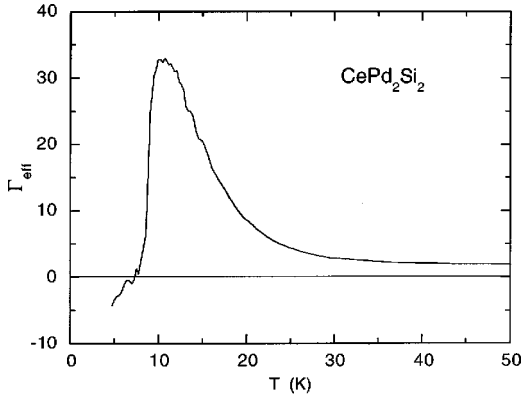

FIG. 11. Effective Grüneisen parameter Γ_{eff} of $CePd_2Si_2$ as a function of temperature.

measurements indicated a value of $c \approx 6.8$ J mol^{-1} K^{-2} for the Schottky anomaly.[24] Using the isothermal compressibility $\kappa = 0.82$ Mbar^{-1} for $CeRu_2Si_2$,[35] we find a Grüneisen parameter of $\Gamma_{CEF} = -9.3$ for the crystal-field splitting of the excited doublets. The negative volume dependence of the crystal-field splitting is strongly anisotropic and predominantly caused by the sensitivity to the *c*-axis lattice parameter. A comparison with the crystal-field splitting of isostructural Ce compounds confirms this trend.[5,36]

2. Spin fluctuations

From the measured specific heat and thermal-expansion curves an effective Grüneisen parameter can be defined as $\Gamma_{\rm eff}(T) = V_m \alpha_v(T)/\kappa c(T)$ (see Fig. 11). The effective Grüneisen parameter is temperature independent if the system can be described by a single energy scale. At high temperatures the effective Grüneisen parameter shows a small constant value of $\Gamma_{ph} = 2$ and describes the volume dependence of the characteristic energy scale for the phonons. Below 30 K the effective Grüneisen parameter rapidly increases and reaches a value of $\Gamma_{eff} = 33$ just above T_N. In the low-temperature limit, $\Gamma_{\rm eff}(T)$ corresponds to the strongly enhanced electronic Grüneisen parameter $\Gamma_{HF} = d \ln \gamma / d \ln V$ ($\approx$40–50) for heavy-fermion systems.

3. Magnetic order

The uniaxial pressure dependence of the transition temperature can be evaluated with the Ehrenfest relation $dT_N/dp_i = V_m \Delta \alpha_i / \Delta(c/T)$. Using the measured anomalies in the coefficients of the thermal expansion $\Delta \alpha_a = -9.4 \times 10^{-6}$ K^{-1} and $\Delta \alpha_c = 9.5 \times 10^{-6}$ K^{-1} in combination with the jump in the specific heat $\Delta(c/T) = 0.60$ J mol^{-1} K^{-2}, we find values of $dT_N/dp_a = -83$ mK/kbar and $dT_N/dp_c = 84$ mK/kbar. The corresponding hydrostatic pressure dependence of the transition temperature amounts to $dT_N/dp = -82$ mK/kbar and is in good agreement with the low-pressure data of recent electrical resistivity measurements under hydrostatic pressures up to 30 kbar.[14] The Grüneisen parameter for T_N is defined as $\Gamma_N = -d \ln T_N / d \ln V \approx -11$.[14] The opposite signs for Γ_N and Γ_{HF} indicates a strong competition of the antiferromagnetic order with the Kondo fluctuations, characteristic for heavy-fermion systems.

TABLE III. Characteristic energy scales of $CePd_2Si_2$ at different pressures. The values under pressure are estimated from the relevant Grüneisen parameters.

p (kbar)	$\Delta_{\rm CEF}$ (K)	T_N (K)	T_K (K)
0	220	8.5	10
28	173	0	18

D. Pressure dependence

Resistivity measurements under hydrostatic pressure showed that the antiferromagnetic order is suppressed at a critical pressure of about 30 kbar.[13–15] Surprisingly, a superconducting transition at $T_c \approx 0.4$ K was observed for pressures around the critical pressure. The effect of pressure on the characteristic energy scales of $CePd_2Si_2$ can be estimated from the experimental values of the Grüneisen parameters. The crystal-field level splitting of $\Delta_{CEF} = 220$ K shows a relatively weak pressure dependence of $d \ln \Delta_{CEF}/dp = \kappa \Gamma_{CEF} \approx -7.6$ Mbar^{-1}. The pressure dependence of the Kondo temperature is determined by the strongly enhanced heavy-fermion Grüneisen parameter of $\Gamma_{HF} = -d \ln T_K / d \ln V = 33$ at T_N. The Kondo temperature shows a strong increase under pressure with $d \ln T_K/dp = \kappa \Gamma_{HF} \approx 27$ Mbar^{-1}. The characteristic energy scales at the critical pressure ($p \approx 28$ kbar) are indicated in Table III and are in qualitative agreement with the general trends for CeT_2Si_2 systems.[3] Under applied pressure the magnetic exchange energy J increases and directly influences the balance between the indirect exchange interaction and the screening of the Ce^{3+} ions. The characteristic energy of the exchange interaction is $T_{\rm RKKY} \sim NJ^2$, while the Kondo screening energy corresponds to $T_K \sim (1/N)\exp(-1/N|J|)$, where N is the electron density of states at the Fermi level. When J approaches the critical value J_c, T_K grows more rapidly than $T_{\rm RKKY}$ and the antiferromagnetic ordering temperature T_N decreases until it vanishes at J_c. An alternative route to reach the quantum critical point is by chemical substitution of one of the elements.[24,37–39] As a general trend the spin fluctuations and the Kondo temperature become strongly enhanced when the antiferromagnetic order is suppressed.

V. CONCLUSIONS

We have studied the magnetic interactions of single-crystalline $CePd_2Si_2$ by measurements of the electrical resistivity, specific heat, thermal expansion, magnetic susceptibility, and elastic and inelastic neutron scattering. In the paramagnetic phase the system is characterized by Kondo-type spin fluctuations, while below T_N the spin fluctuations coexist with spin-wave excitations. The spin waves are strongly dispersive, with a minimum energy of 0.83 meV at the magnetic zone center $\mathbf{k} = (1/2,1/2,0)$. The dispersion can be described in terms of a two-sublattice model with a reduced magnetic exchange interaction and a strong damping of the spin waves due to Kondo screening. The volume dependence of the magnetic interactions has been analyzed

using the Grüneisen parameters and is found to be strongly anisotropic.

ACKNOWLEDGMENTS

We gratefully acknowledge the numerous contributions to the present measurements by I. Sheikin (resistivity), R. Calemczuk (specific heat), A. de Visser and P. Haen (thermal expansion), and B. Hennion (neutron scattering). Part of the neutron-scattering measurements was carried out at the Laboratoire Léon Brillouin at CEA Saclay, Laboratoire Commun CEA-CNRS. We have benefited from discussions with J. Flouquet and S. Raymond.

[1] S. Doniach, Physica B **91**, 231 (1977).
[2] M. A. Continentino, Phys. Rev. B **47**, 11 587 (1993).
[3] T. Endstra, G. J. Nieuwenhuys, and J. A. Mydosh, Phys. Rev. B **48**, 9595 (1993).
[4] V. Murgai, S. Raaen, L. C. Gupta, and R. D. Parks, in *Valence Instabilities*, edited by P. Wachter and H. Boppart (North-Holland, Amsterdam, 1982), p. 537.
[5] A. Severing, E. Holland-Moritz, B. D. Rainford, S. R. Culverhouse, and B. Frick, Phys. Rev. B **39**, 2557 (1989).
[6] R. A. Steeman, T. E. Mason, H. Lin, W. J. L. Buyers, A. A. Menovsky, M. F. Collins, E. Frikkee, G. J. Nieuwenhuys, and J. A. Mydosh, J. Appl. Phys. **67**, 5203 (1990).
[7] B. H. Grier, J. M. Lawrence, V. Murgai, and R. D. Parks, Phys. Rev. B **29**, 2664 (1984).
[8] R. A. Steeman, E. Frikkee, R. B. Helmholdt, A. A. Menovsky, J. van der Berg, G. J. Nieuwenhuys, and J. A. Mydosh, Solid State Commun. **66**, 103 (1988).
[9] A. Severing, E. Holland-Moritz, and B. Frick, Phys. Rev. B **39**, 4164 (1989).
[10] B. H. Grier, J. M. Lawrence, V. Murgai, and R. D. Parks, J. Phys. C **21**, 1099 (1988).
[11] M. Loewenhaupt and K. H. Fischer, in *Handbook on the Physics and Chemistry of Rare Earths*, Vol. 16, edited by K. A. Gschneidner, Jr. and L. Eyring (North-Holland, Amsterdam, 1993), p. 51.
[12] J. D. Thompson, R. D. Parks, and H. Borges, J. Magn. Magn. Mater. **54-57**, 377 (1986).
[13] F. M. Grosche, S. R. Julian, N. D. Mathur, and G. G. Lonzarich, Physica B **223-224**, 50 (1996).
[14] S. R. Julian, C. Pfleiderer, F. M. Grosche, N. D. Mathur, G. J. McMullan, A. J. Diver, I. R. Walker, and G. G. Lonzarich, J. Phys.: Condens. Matter **8**, 9675 (1996); S. R. Julian, F. V. Carter, F. M. Grosche, R. K. W. Haselwimmer, S. J. Lister, N. D. Mathur, G. J. McMullan, C. Pfleiderer, S. S. Saxena, I. R. Walker, N. J. W. Wilson, and G. G. Lonzarich, J. Magn. Magn. Mater. **177-181**, 265 (1998).
[15] S. Raymond and D. Jaccard, Phys. Rev. B **61**, 8679 (2000).
[16] N. D. Mathur, F. M. Grosche, S. R. Julian, I. R. Walker, D. M. Freye, R. K. W. Haselwimmer, and G. G. Lonzarich, Nature (London) **394**, 39 (1998).
[17] Z. Fisk and D. Pines, Nature (London) **394**, 22 (1998).
[18] A. J. Millis, Phys. Rev. B **48**, 7183 (1993).
[19] T. Moriya and T. Takimoto, J. Phys. Soc. Jpn. **64**, 960 (1995).
[20] M. A. Continentino, Z. Phys. B: Condens. Matter **101**, 197 (1996).
[21] P. Lejay, J. Muller, and R. Argoud, J. Cryst. Growth **130**, 238 (1993).
[22] F. Hippert, B. Hennion, J. M. Mignot, and P. Lejay, J. Magn. Magn. Mater. **108**, 177 (1992).
[23] P. Link, D. Jaccard, and P. Lejay, Physica B **223-224**, 303 (1996).
[24] M. J. Besnus, A. Braghta, and A. Meyer, Z. Phys. B: Condens. Matter **83**, 207 (1991).
[25] A. de Visser, Ph.D. thesis, University of Amsterdam, 1986.
[26] Y. Kawasaki, K. Ishida, Y. Kitaoka, and K. Asayama, Phys. Rev. B **58**, 8634 (1998).
[27] S. W. Lovesey, *Theory of Neutron Scattering from Condensed Matter* (Oxford University Press, Oxford, 1984), Vol. 2, pp. 109–114.
[28] N. H. van Dijk, B. Fåk, T. Charvolin, P. Lejay, J. M. Mignot, and B. Hennion, Physica B **241-243**, 808 (1998).
[29] K. W. H. Stevens, Proc. Phys. Soc., London, Sect. A **65**, 209 (1952).
[30] M. T. Hutchings, in *Solid State Physics: Advances in Research and Applications*, edited by F. Seitz and B. Turnbull (Academic, New York, 1965), Vol. 16, p. 227.
[31] H. Abe, H. Kitazawa, H. Suzuki, G. Kido, and T. Matsumoto, J. Magn. Magn. Mater. **177-181**, 479 (1998).
[32] Ref. 22 contains a printing error: the correct crystal-field parameters should be $B_2^0 = -0.36$ meV, $B_4^0 = 0.02$ meV, and $B_4^4 = 0.355$ meV for an isotropic molecular field of $\lambda = -30$ mol/emu.
[33] H. Abe, H. Kitazawa, H. Suzuki, G. Kido, and T. Matsumoto, Physica B **246-247**, 141 (1998).
[34] N. H. van Dijk, F. Bourdarot, J. C. P. Klaasse, I. H. Hagmusa, E. Brück, and A. A. Menovsky, Phys. Rev. B **56**, 14 493 (1997).
[35] P. Haen, J. M. Laurant, K. Payer, and J. M. Mignot, in *Transport and Thermal Properties of f-Electron Systems*, edited by G. Oomi *et al.* (Plenum, New York, 1993), p. 145.
[36] A. Loidl, K. Knorr, G. Knopp, A. Krimmel, R. Caspary, A. Böhm, G. Sparn, C. Geibel, F. Steglich, and A. P. Murani, Phys. Rev. B **46**, 9341 (1992).
[37] M. J. Besnus, A. Braghta, P. Haen, J. P. Kappler, and A. Meyer, Physica B **206-207**, 295 (1995).
[38] T. Kusumoto, S. Takagi, and H. Suzuki, Physica B **206-207**, 301 (1995).
[39] M. Gömez Berisso, O. Trovarelli, P. Pedrazzini, G. Zwicknagl, C. Geibel, F. Steglich, and J. G. Sereni, Phys. Rev. B **58**, 314 (1998); M. Gómez Berisso, P. Pedrazzini, J. G. Sereni, O. Trovarelli, C. Geibel, and F. Steglich, Physica B **259-261**, 68 (1999).